Check for updates

The effect of CO$_2$ loading on alkanolamine absorbents in aqueous solutions†

Sergey M. Melnikov and Matthias Stein [ID] *

Post-combustion carbon capture by amine scrubbing is the most frequently used process to remove CO$_2$ from pulverized coal-fired power plants and also biogas flue gas streams. The quest for novel absorbents for CO$_2$ capture with improved properties requires insight into the properties of the CO$_2$-loaded mixed solutions. A comparative molecular dynamics study of the product state solutions, with chemically-bound CO$_2$ of standard monoethanolamine (MEA) and the new alternative 4-diethylamino-2-butanol (DEAB) at various CO$_2$-loadings yields solvent properties in good agreement with experimental data. The concentration of all post-reaction species in solution was based on experimental equilibria distributions. The data generated provide detailed insight into the properties of reactive mixed alkanolamine solutions. The liquid structure of aqueous MEA solutions undergoes only minor changes when absorbing CO$_2$. The diffusion coefficients of all molecular species, however, decrease significantly with increasing CO$_2$-loadings. The large hydrophobic clusters formed in the reactant state by DEAB molecules in water prior to CO$_2$ binding significantly decrease in size and structure upon CO$_2$ absorption. The diffusion coefficients of all components decrease with increasing CO$_2$-loading, whereas the pre-reaction alkanolamine DEAB shows an increase in diffusion coefficient. This structural and kinetic information supports the molecular design and further development of novel compounds and provides data for a global process simulation and optimization.

Introduction

The post-combustion removal of carbon dioxide from flue gas streams of pulverized coal-fired power plants and also biogas from anaerobic fermentation require efficient, robust and selective chemical CO$_2$ absorbing compounds.[1–4] Complementing engineering studies, computational approaches are essential to reveal the underlying reaction mechanisms of CO$_2$ absorption and to develop new absorbing compounds.[5,6] Selectivity and reversibility of the absorbent, and its liquid structure properties such as diffusion coefficient and viscosities are important selection criteria. In computational solvent design, molecular dynamics (MD) simulations are able to yield information, which are difficult or sometimes impossible to obtain experimentally. For example, the diffusion coefficient of CO$_2$ in absorbing amine solution cannot be measured due to its reactivity and has to be extracted from nitrous oxide experiments. Recently, a wealth of information about liquid structure, intermolecular interactions and diffusion properties of aqueous alkanolamines, as well as

solvation and mobility of CO$_2$ molecules within such solvents was obtained computationally.[7–18] However, all these studies were limited to the investigation of the pre-reaction state of CO$_2$ in aqueous amine solutions. During the chemical CO$_2$ absorption, carbamate and carbonate ions together with protonated alkanolamines are formed as products of the amine reaction with CO$_2$, which then would eventually change the complex mixed solvent properties. In addition, at increasing CO$_2$ loadings both non-reacted carbon dioxide and partially reacted solvents are present. The design and control of such a chemical absorption process requires information about the solvent properties changes during the reaction. Data about pre-reaction solvents are scarce in comparison to unreacted solvents. The kinetic network modelling CO$_2$ in aqueous alkanolamine solutions requires accurate diffusion coefficients of all solvent components present in solution.[19–21] Experimental viscosity studies of individual constituents do not allow an extrapolation of diffusion coefficients to the reactive solution. Therefore, structure-based simulations are indispensable to provide these missing data and only classical MD simulations allow a sufficient sampling and averaging over long trajectories and a large number of particles to give accurate results.

We here present results from MD studies of CO$_2$-loaded aqueous alkanolamine compounds which were identified from a large screening of candidates.[22] Here, we focus on the primary

Molecular Simulations and Design Group, Max Planck Institute for Dynamics of Complex Technical Systems, Sandtorstrasse 1, 39106 Magdeburg, Germany.
E-mail: matthias.stein@mpi-magdeburg.mpg.de

monoethanolamine (MEA), the standard compound currently mostly used for CO_2 capture, and the novel tertiary alkanolamine 4-diethylamino-2-butanol (DEAB) which were both fully characterized in binary aqueous alkanolamine solutions[14] and in the presence of CO_2.[17] The choice of these two compounds is motivated by their difference in mechanism upon CO_2 absorption and the formation of different intermediates in solution. MEA is fully hydrated and when chemically absorbing one CO_2 molecule the carbamate anion $MEACOO^-$ and the protonated $MEAH^+$ are generated.[23] This sets the upper limit for a maximum capacity of MEA to 0.5 (*i.e.* the ratio of absorbed CO_2 and reacted MEA molecules).[24] DEAB molecules, on the other hand, form large hydrophobic clusters in aqueous solution and during absorption of CO_2 the tertiary amine DEAB deprotonates water to give the protonated DEAB ($DEABH^+$) species, and the hydroxide ion reacts with carbon dioxide to give bicarbonate (HCO_3^-), and carbonate (CO_3^{2-}) ions.[25,26] This sets the maximum capacity of DEAB to 1 (one bicarbonate ion HCO_3^- and one protonated $DEABH^+$ per CO_2 molecule are being formed). Artificial neural network based models were successfully applied to obtain equilibrium solubilities and mass transfer coefficients of CO_2 absorption in aqueous solutions of DEAB[27] from experimental data.[28] and to develop a modeling-optimization framework in order to assess the CO_2 absorption capacity for novel amine solutions.[29] The molecular compounds in equilibrium are a mixture of reactant and product species and are presented in Fig. 1. Liquid structure properties of MEA and DEAB CO_2 absorbents in solution were determined in the product states over a wide range of CO_2-loadings. This reveals the influence of increasing concentrations of post-reaction molecular species on the structure of the complex mixed five- and six-component mixed solution. Changes in solution viscosities and molecular diffusion constants during the chemical absorption process can be traced and give detailed molecular insight into the post-combustion capture of carbon dioxide.

Simulation details

All non-bonded and bonded interactions for alkanolamine molecules, their protonated forms $MEAH^+$ and $DEABH^+$ and the $MEACOO^-$ carbamate and also (bi-)carbonate ions were treated with help of the all-atom optimized potentials for liquid simulations (OPLS-AA) forcefield.[30] Water molecules were represented by the charge/extended (SPC/E) model,[31] and CO_2 molecules by the transferable potentials for the phase equilibria (TraPPE).[32] The accuracy of the use of these forcefields for the simulation of CO_2 solvation in aqueous alkanolamines was validated before.[14,17] Partial charges for the carbamate $MEACOO^-$ and protonated $MEAH^+$ were taken from literature,[18] and for the protonated $DEABH^+$ from ref. 30. For a consistent set of charges, the Lowdin atomic charges for HCO_3^- and CO_3^{2-} were re-calculated with Jaguar v. 8.7,[33] using the M06-2 hybrid functional,[34] an implicit SM8 solvation model for water[35,36] and a 6-31G*+ basis set for all atoms. The charge distribution was symmetrized for chemically equivalent atoms and retains
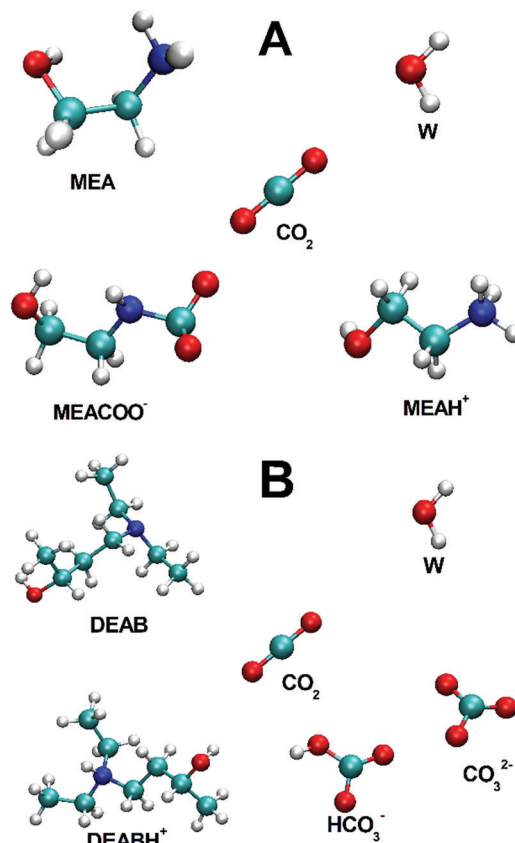

Fig. 1 Molecular species in post-reaction mixed alkanolamine solutions: (A) five-component $MEA/MEAH^+/MEACOO^-/H_2O/CO_2$ system, (B) six-component $DEAB/DEABH^+/H_2O/CO_2/HCO_3^-/CO_3^{2-}$ solution.

the full molecular charge. The calculated partial charges are given in the ESI.† Long-range electrostatic interactions were treated with the particle-mesh Ewald algorithm. Non-bonded interactions were modeled with a 12-6 Lennard-Jones potential. A cutoff radius of 1.4 nm was used for all interactions. Lennard-Jones parameters for unlike interactions were calculated using the geometric average rule. MD simulations were carried out with Gromacs 5.1.2[37] at 313 K. An isothermal–isobaric (*NPT*) ensemble 2 ns simulation run (preceded by 500 ps of equilibration) was carried out to define the solvent density. The liquid solution structures and molecular diffusion coefficients were acquired in a canonical (*NVT*) ensemble 40 ns simulation run (preceded by a 1 ns equilibration run). Such long trajectories were needed in order to obtain reliable and converged results for the diffusion coefficient of CO_2 molecules at a low concentration of 0.1 M. The number of molecules and simulation box sizes for all studied molecular ensembles are provided in the ESI† (Tables S1 and S2). The appropriate simulation box dimensions were checked for absence of finite size effects. Diffusion coefficients were calculated from the relation between the mean square displacement and the observation time (over a 100–500 ps time interval).[38] The shear viscosities were calculated using the non-equilibrium method[39] by applying external forces, from which the energy is dissipated through viscous friction. The generated heat is removed by coupling to a heat bath.

Results and discussion

Simulations were carried out for starting compositions of alkanolamine/water solvent ratios of 30/70 w/w MEA/W and 22.5/77.5 w/w DEAB/W which are typical for the absorption process[2,4] and at a typical process temperature of 313 K.[22,40] The mole fractions of species in mixed solutions at various CO_2 loadings were obtained from NMR spectroscopic studies.[41,42] The absolute compositions for each system are given in the ESI† (Tables S1 and S2). A comparison with experimental[43,44] data such as densities and viscosities is given in Fig. 2. There is a very good agreement for liquid densities over the entire range of CO_2 loading (deviations are below 1% for MEA and 2.5% for DEAB). The calculated viscosities are also in good agreement with experiment and correctly reproduce the trend of increasing viscosities with increasing loading. According to our findings, the TIP4P/2005 water model[45] performs slightly better for solvent viscosities of DEAB, but less so for the diffusion coefficients of complex mixed aqueous alkanolamine solutions.[14] The large changes in density and viscosity with CO_2 loading for MEA with respect to DEAB can be rationalized by the fact that the number of absorbed CO_2 molecules in MEA at 0.5 loading is about 2 times larger than that in DEAB even at 0.815 loading.

In CO_2-loaded solution, the primary amine MEA molecules are fully solvated by water and the CO_2 molecules are equally distributed between water and alkanolamine molecules.[17] A simulation snapshot of an entire system at 0.3 CO_2-loading is provided in Fig. S1 (ESI†). Compared to the pre-reaction system at 0 loading, in the fully reacted product system the MEA–MEA
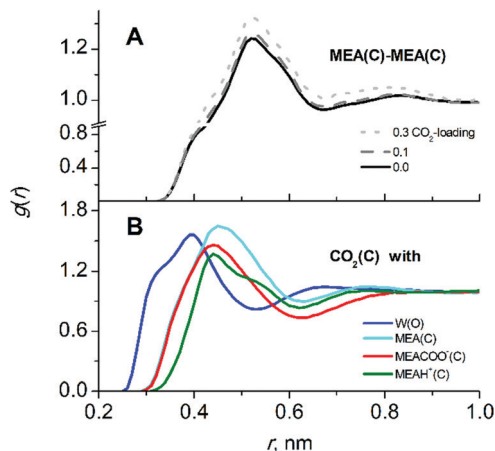

Fig. 3 Liquid solution structure of the five-component CO_2-loaded aqueous MEA. (A) Radial distribution functions (RDFs) of alkanolamines MEA–MEA interactions at various CO_2 loadings, (B) RDFs for CO_2 interacting with all other molecular species (W/MEA/MEAH$^+$/MEACOO$^-$) in solution at 0.3 loading at which all reaction products are present in significant amount.

(see Fig. 3A), MEA–CO_2 (see the Fig. S3, ESI†) and likewise the MEA–water interactions are only marginally affected by increase of CO_2-loading. The slight increase of the first and second peak amplitudes in the radial distribution function (RDF) of MEA$_{C–C}$ (first and second solvation shells) at increasing CO_2-loading is an evidence for a small increase of the mutual aggregation of MEA molecules. This feature can be rationalized by an increase of self-association of the more hydrophobic MEA molecules separating from the MEACOO$^-$ and MEAH$^+$ ionic species and polar water molecules. MEACOO$^-$ and MEAH$^+$ form a persistent ion pair in solution with only an occasional exchange of molecules. The characteristic lifetime for the ion pair is about 100 ps across the entire range of CO_2-loading. The strong MEACOO$^-$–MEAH$^+$ pair is fully solvated by water molecules, uniformly distributed in solution and does not form larger clusters. As an example for the charged species interactions in the mixed five-component system, the RDF of the carbamate MECOO$^-$ with the other species in solution is given in Fig. 4.

The RDFs for the interactions of MEA and MEAH$^+$s with other compounds in solution are given in the ESI.†

The solvation of CO_2 in MEA solutions is not significantly affected by increasing the CO_2-loading. The RDFs of CO_2 inter-actions with other molecular species in solution at 0.3 loading are shown in Fig. 3B. As also found in the pre-reaction state, CO_2 is equally found in proximity of water and MEA molecules (similar peak heights in Fig. 3B) but only slightly less probable to interact with MEACOO$^-$ and MEAH$^+$. Analysis of interactions between CO_2–MEA molecules at different loadings is given in the ESI† (Fig. S3). Upon an increase of MEACOO$^-$–MEAH$^+$ pair formation at higher CO_2-loadings, the presence of CO_2 molecules close to MEA species also increases slightly (see Fig. S3, ESI†).

Fig. 5 shows the molecular diffusion coefficients of all species present in solution after covalent CO_2 binding to MEA. The diffusion coefficients of all species significantly decrease with increasing CO_2-loading (numerical data can be found in the ESI,† Table S4). It has to be noted that the diffusion
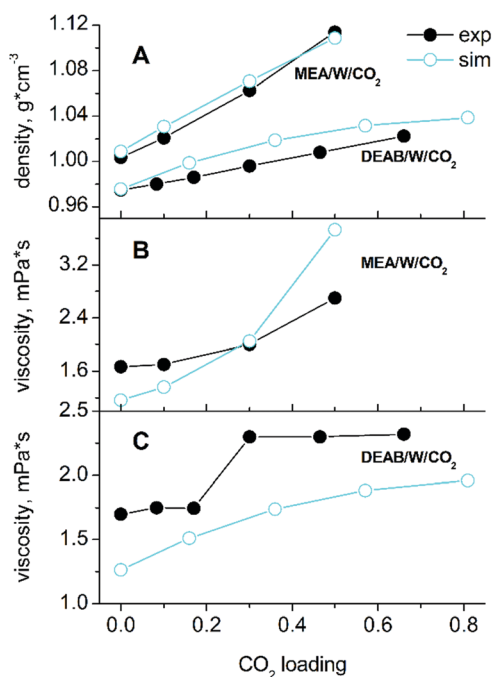

Fig. 2 Comparison of liquid state properties with experiments at T = 313 K. Panel (A) shows the densities of the five- and six-component mixed solvents, panels (B) and (C) display the viscosities of the MEA/MEAH$^+$/MEACOO$^-$/W/CO_2 and DEAB/DEABH$^+$/W/CO_2/HCO$_3^-$/CO$_3^{2-}$ systems as a function of CO_2-loading.
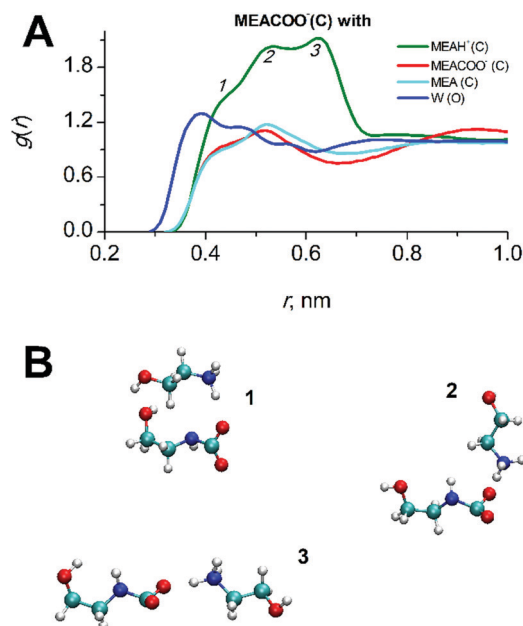
Fig. 4 RDFs of interactions of the carbamate $MEACOO^-$ with other mixture species at a CO_2-loading of 0.3. The peaks numbered 1, 2, 3 at the top panel (A) refer to the long living $MEACOO^- - MEAH^+$ species shown on the bottom panel (B).
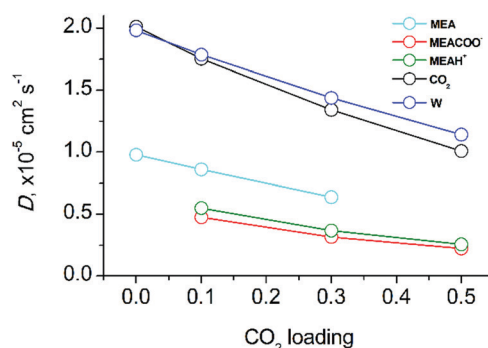

Fig. 5 Diffusion coefficients of molecular components as a function of CO_2 loading in aqueous MEA/CO_2 solution.

coefficient of CO_2 in the fully reacted system (at 0.5 loading) is two times smaller than in the pre-reaction state since all MEA molecules have reacted with CO_2. As expected, the mobility is critically dependent on the molecular mass: the heaviest molecules $MEACOO^-$ and $MEAH^+$ are least mobile whereas water and CO_2 diffuse fastest. The significant decrease of molecular diffusion coefficients is consistent with the experimentally measured increase of viscosity of the mixed solution (see above). Since hydrogen bond formation of water molecules does not change with CO_2-loading (data not shown), the increase of viscosity of CO_2-loaded MEA solution can only be explained by an increase of ion pair formation of $MEACOO^-$ and $MEAH^+$ with higher supramolecular masses and lower diffusion coefficients.

Compared to the primary amine MEA, the tertiary amine DEAB displays a different behavior upon an increase of CO_2 loading. In the pre-react state, DEAB molecules tend to self-aggregate and
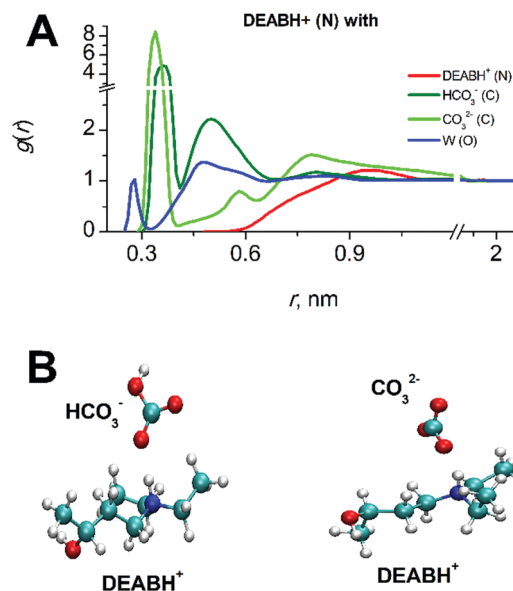

Fig. 6 (A) Molecular interactions of $DEABH^+$ in the partially reacted mixed of solution $DEAB/W/CO_2$ with other species at a CO_2-loading of 0.364. (B) Simulation snapshots displaying the most frequently occurring conformations of interactions in $DEABH^+/HCO_3^-$ and $DEABH^+/CO_3^{2-}$ ion pairs.

form large clusters (see a snapshot of an entire system in Fig. S2, ESI†). The CO_2 molecules show a preferred localization within these hydrophobic aggregates.[14,17]

In contrast to MEA, absorption of CO_2 in aqueous solutions by DEAB significantly affects the liquid structure. The effect of increasing CO_2 loading on DEAB cluster formation can be seen in Fig. 6A. The peak amplitudes of the first and the second peaks of the RDF characterize the tendency of DEAB molecules to form self-aggregates. At low CO_2-loading, DEAB clustering even increases since the presence of only a small amount of charged particles $DEABH^+/HCO_3^-/CO_3^{2-}$ in solution enhances the hydrophobic/hydrophilic phase separation. Upon further increase of CO_2-loading, more DEAB molecules have participated in the chemical reaction with CO_2 which then leads to the formation of an increasing number of protonated $DEABH^+$ molecules. Those tend to separate from the DEAB clusters due to their hydrophilic character and the number of hydrophobic DEAB–DEAB interactions decreases. This can be seen by the decrease of peak amplitudes in Fig. 6A at high loading. At a CO_2-loading of 0.815, the second solvation shell of DEAB–DEAB aggregates almost vanishes indicating the formation of isolated molecular clusters.

The product $DEABH^+$ molecules form strong and stable complexes with oppositely charged HCO_3^- and CO_3^{2-} species (see Fig. 7). The lifetime of such an electrostatic interaction is about 100 ps for the $DEABH^+$–bicarbonate and 1–1.5 ns for the $DEABH^+$–CO_3^{2-} pair. The ionic ion pairs are uniformly distributed within each solution.

The localization of CO_2 molecules in close proximity to DEAB nitrogen atoms follows the same tendency as the DEAB–DEAB interactions upon increasing CO_2-loadings. At low loading, the local CO_2 enrichment increases while with further CO_2-loading it

This journal is © the Owner Societies 2019

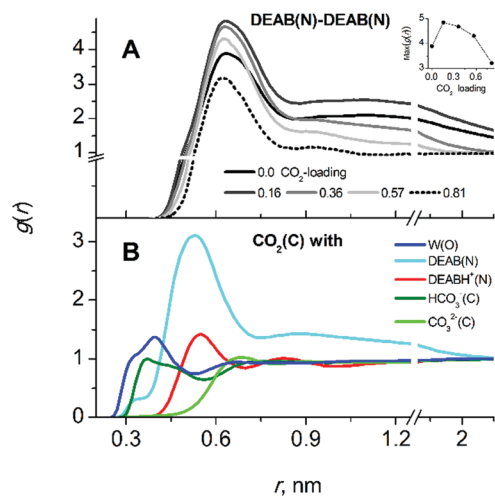*Phys. Chem. Chem. Phys.*, 2019, **21**, 18386–18392 | 18389

Fig. 7 Intermolecular interactions in CO_2-loaded aqueous DEAB solution. (A) RDFs of hydrophobic DEAB(N)–DEAB(N) at increasing CO_2 loadings. (B) CO_2 interactions with water, $DEABH^+$, HCO_3^- and CO_3^{2-} at a loading of 0.364.

starts to decrease and finally disappears (see the CO_2–DEAB RDFs in the Fig. S6, ESI†). This can be rationalized when considering the decrease of unreacted DEAB molecules in number at higher CO_2-loading. Thus, the molecular clusters of DEAB become smaller in size, water molecules are beginning to penetrate these clusters and displace CO_2 molecules close to the amine nitrogen atoms. The CO_2–DEAB interaction is clearly the most prevalent and CO_2 interactions with water, $DEABH^+$, HCO_3^- and CO_3^{2-} (see Fig. 6B) are less prominent. This is due to the hydrophobic nature of the interaction between CO_2 and the alkanolamine solvent.[17]

Fig. 8 shows the diffusion coefficients of all molecular species in DEAB at various loadings (for numerical data see Table S5 in the ESI†). With increasing CO_2-loading, the mobility of all compounds in the mixed solutions decreases. This is in agreement with the observed increase of viscosity (see above). The diffusion coefficients for $DEABH^+$ and CO_3^{2-} are identical expect for very high loading when the strong electrostatic interaction is persistent (with a lifetime of 1 ns) and the complex
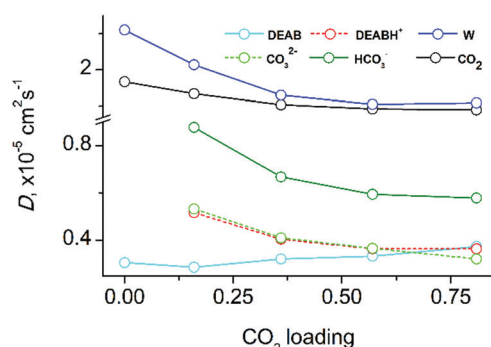

Fig. 8 Diffusion coefficients of reaction product species in equilibrium as a function of CO_2 loading in the six-component mixture of aqueous DEAB with CO_2.

diffuses as a supermolecule. At low and intermediate CO_2 loadings, the carbonate ions are preferably solvated by water molecules. The electrostatic interaction between the bicarbonate HCO_3^- and $DEABH^+$ is weaker and thus it shows a faster diffusion. The slower diffusion of CO_3^{2-} ions is determined its larger charge due to which the interactions with surrounding water molecules and $DEABH^+$ are stronger and responsible a slower mobility.

The hydrophobic DEAB molecules within the self-aggregate clusters diffuse slower than charged $DEABH^+$ molecules even when the latter are bound to anionic species such as carbonate and bi-carbonate. At very low CO_2-loading, the DEAB molecules move even slower than in case of the pre-reaction solvent. As the CO_2-loading increases, the DEAB cluster size becomes smaller and the diffusion coefficients of DEAB molecules thus increase with CO_2 concentration and finally approach that of $DEABH^+$. The free CO_2 molecules are mostly localized within the DEAB clusters and are moving much faster than the DEAB molecules. The load-dependence of CO_2 diffusion reflects on the one hand the acceleration of DEAB molecule diffusion and on the other hand the slower diffusion of other species in solution. Therefore, the CO_2 diffusion coefficient is less sensitive to the CO_2-loading than other mixture components. At a maximum loading of 0.815, the CO_2 diffusion coefficient is still at 79% of the non-reacted ternary system. Water diffusion slows down upon increase of CO_2 loading since the number of charged species $DEABH^+/HCO_3^-/CO_3^{2-}$ increased which possess a tight solvation shell.

Conclusions

In conclusion, MD studies of CO_2-loaded aqueous alkanolamine solutions for two representatives (MEA and DEAB solvents) were performed over a broad range of loading. Reaction of carbon dioxide with alkanolamines leads to complex five- and six-component post-reaction mixed solutions with different behavior.

CO_2 absorption does not significantly alter the liquid structure properties but the molecular diffusion coefficients change significantly for the standard primary amine MEA in aqueous solution. The MEA molecules and all charged product species are individually solvated; CO_2 shows no preference to approach either MEA or water molecules. The diffusion coefficients of all molecule species decrease with increasing CO_2-loading since the number of charged species and the solvent viscosity increase during the reaction.

For the tertiary alkanolamine DEAB, an opposite behavior is observed. Self-aggregation and clustering of hydrophobic DEAB molecules are diminishing in presence of the newly formed charged and hydrophilic absorbent species; the local concentration of CO_2 molecules decreases in vicinity of DEAB molecules. At increasing CO_2-loading, the diffusion coefficients decrease for all species in solution except for unreacted DEAB. Their mobility increases and finally approaches that of the protonated $DEABH^+$ product. The change of diffusion coefficient of CO_2 at increasing load is less prominent due to two

18390 | *Phys. Chem. Chem. Phys.*, 2019, **21**, 18386–18392

This journal is © the Owner Societies 2019

compensating effects: the acceleration of mobility of the first solvation shell CO_2 molecules in close proximity to DEAB molecules at low loading and the disruption of DEAB self-aggregates at higher loadings.

A clear understanding of molecular processes during carbon dioxide sequestration in post-combustion capture is an important pre-requisite to design and control novel CO_2 absorbing compounds. The results show that different, sometimes competing effects have an influence on the diffusional properties and viscosities of amine scrubbers in reactors at different CO_2 loadings. The physical and organic chemistry of alkanolamines is not facile to rationalize and requires careful analysis of novel data from structure-based simulations. These generated data form the basis of global process simulations and optimization of the entire carbon dioxide sequestration process in a chemical engineering approach.

Conflicts of interest

The authors declare no competing financial interest.

Acknowledgements

References

1 G. T. Rochelle, *Science*, 2009, **325**, 1652–1654.

2 B. Dutcher, M. Fan and A. G. Russell, *ACS Appl. Mater. Interfaces*, 2015, **7**, 2137–2148.

3 D. M. D'Alessandro, B. Smit and J. R. Long, *Angew. Chem., Int. Ed.*, 2010, **49**, 6058–6082.

4 Z. Liang, W. Rongwong, H. Liu, K. Fu, H. Gao, F. Cao, R. Zhang, T. Sema, A. Henni, K. Sumon, D. Nath, D. Gelowitz, W. Srisang, C. Saiwan, A. Benamord, M. Al-Marrid, H. Shi, T. Supap, C. Chan, Q. Zhou, M. Abu-Zahra, M. Wilson, W. Olson, R. Idem and P. Tontiwachwuthikul, *Int. J. Greenhouse Gas Control*, 2015, **40**, 26–54.

5 H. M. Stowe and G. S. Hwang, *Ind. Eng. Chem. Res.*, 2017, **56**, 6887–6899.

6 X. Yang, R. J. Rees, W. Conway, G. Puxty, Q. Yang and D. A. Winkler, *Chem. Rev.*, 2017, **117**, 9524–9593.

7 F. Moosavi, F. Abdollahi and M. Razmkhah, *Int. J. Greenhouse Gas Control*, 2015, **37**, 158–169.

8 Y. S. Yu, H. F. Lu, G. X. Wang, Z. X. Zhang and V. Rudolph, *J. Chem. Eng. Data*, 2013, **58**, 1429–1439.

9 Y. H. Jhon, J. G. Shim, J. H. Kim, J. H. Lee, K. R. Jang and J. Kim, *J. Phys. Chem. A*, 2010, **114**, 12907–12913.

10 L. V. H. M. Stowe, E. Paek and G. S. Hwang, *Phys. Chem. Chem. Phys.*, 2015, **17**, 29184–29192.

11 E. F. Da Silva, T. Kuznetsova, B. Kvamme and K. M. Merz Jr, *J. Phys. Chem. B*, 2007, **111**, 3695–3703.

12 S. A.-I. M. Narimani and H. Modarress, *J. Nat. Gas Sci. Eng.*, 2017, **47**, 154–166.

13 I. S. Huang, J. J. Li and M. K. Tsai, *Molecules*, 2017, **22**, 8.

14 S. M. Melnikov and M. Stein, *J. Phys. Chem. B*, 2018, **122**, 2769–2778.

15 G. A. Orozco, V. Lachet and A. D. Mackie, *Mol. Simul.*, 2014, **40**, 123–133.

16 A. V. Gubskaya and P. G. Kusalik, *J. Phys. Chem. A*, 2004, **108**, 7165–7178.

17 S. M. Melnikov and M. Stein, *ACS Sustainable Chem. Eng.*, 2019, **7**, 1028–1037.

18 Q. Chen, S. P. Balaji, M. Ramdin, J. J. Gutiérrez-Sevillano, A. Bardow, E. Goetheer and T. J. H. Vlugt, *Ind. Eng. Chem. Res.*, 2014, **53**, 18081–18090.

19 K. R. Putta, H. Knuutila and H. F. Svendsen, *Energy Procedia*, 2014, **114**, 1576–1583.

20 M. E. T. Sema, A. Naami, R. Idem and P. Tontiwachwuthikul, *Ind. Eng. Chem. Res.*, 2012, **51**, 925–930.

21 M. Afkhamipour and M. Mofarahi, *RSC Adv.*, 2017, **7**, 17857–17872.

22 A. I. Papadopoulos, S. Badr, A. Chremos, E. Forte, T. Zarogiannis, P. Seferlis, S. Papadokonstantakis, A. Galindo, G. Jackson and C. S. Adjiman, *Mol. Syst. Des. Eng.*, 2016, **1**, 313–334.

23 D. E. Penny and T. J. Ritter, *J. Chem. Soc., Perkin Trans. 1*, 1983, 2103.

24 A. G. H. Wee, G.-J. Fan, R. Idem and P. Tontiwachwuthikul, *Ind. Eng. Chem. Res.*, 2009, **48**, 2717–2720.

25 T. L. Donaldson and Y. N. Nguyen, *Ind. Eng. Chem. Fundam.*, 1980, **19**, 260–266.

26 E. B. Rinker, S. A. Sami and O. C. Sandall, *Chem. Eng. Sci.*, 1995, **50**, 755–768.

27 S. Meesattham, P. Charoensiritanasin, S. Ongwattanakul, Z. Liang, P. Tontiwachwuthikul and T. Sema, *Petroleum*, 2019, DOI: 10.1016/j.petlm.2018.09.005.

28 T. Sema, A. Naami, R. Idem and P. Tontiwachwuthikul, *Ind. Eng. Chem. Res.*, 2011, **50**, 14008–14015.

29 M. Afkhamipour and M. Mofarahi, *J. Cleaner Prod.*, 2018, **171**, 234–249.

30 W. L. Jorgensen, D. S. Maxwell and J. Tirado-Rives, *J. Am. Chem. Soc.*, 1996, **118**, 11225–11236.

31 H. J. C. Berendsen, J. R. Grigera and T. P. Straatsma, *J. Phys. Chem.*, 1987, **91**, 6269–6271.

32 J. I. Siepmann and J. J. Potoff, *AIChE J.*, 2001, **47**, 1676–1682.

33 A. D. Bochevarov, E. Harder, T. F. Hughes, J. R. Greenwood, D. A. Braden, D. M. Philipp, D. Rinaldo, M. D. Halls, J. Zhang and R. A. Friesner, *Int. J. Quantum Chem.*, 2013, **113**, 2110–2142.

34 Y. Zhao and D. G. Truhlar, *Theor. Chem. Acc.*, 2008, **120**, 215–241.

35 A. V. Marenich, R. M. Olson, C. P. Kelly, C. J. Cramer and D. G. Truhlar, *J. Chem. Theory Comput.*, 2007, **3**, 2011–2033.

36 R. M. Olson, A. V. Marenich, C. J. Cramer and D. G. Truhlar, *J. Chem. Theory Comput.*, 2007, **3**, 2046–2054.

37 M. J. Abraham, T. Murtola, R. Schulz, S. Páll, J. C. Smith, B. Hess and E. Lindah, *SoftwareX*, 2015, **1-2**, 19–25.

This journal is © the Owner Societies 2019

Phys. Chem. Chem. Phys., 2019, **21**, 18386–18392 | 18391

38 S. M. Melnikov, A. Höltzel, A. Seidel-Morgenstern and U. Tallarek, *J. Phys. Chem. C*, 2016, **120**, 13126–13138.

39 B. Hess, *J. Chem. Phys.*, 2002, **116**, 209–217.

40 A. L. Kohl and R. B. Nielsen, in *Gas Purification*, ed. A. L. Kohl and R. B. Nielsen, Gulf Professional Publishing, Houston, 5th edn, 1997, pp. 40–186.

41 W. Böttinger, M. Maiwald and H. Hasse, *Fluid Phase Equilib.*, 2007, **263**, 131–143.

42 H. Shi, T. Sema, A. Naami, Z. Liang, R. Idem and P. Tontiwachwuthikul, *Ind. Eng. Chem. Res.*, 2012, **51**, 8608–8615.

43 T. G. Amundsen, L. E. Øi and D. A. Eimer, *J. Chem. Eng. Data*, 2009, **54**, 3096–3100.

44 F. Pouryousefi, R. Idem, T. Supap and P. Tontiwachwuthikul, *Ind. Eng. Chem. Res.*, 2016, **55**, 11614–11621.

45 J. L. Abascal and C. Vega, *J. Chem. Phys.*, 2005, **123**, 234505.

18392 | *Phys. Chem. Chem. Phys.*, 2019, **21**, 18386–18392

This journal is © the Owner Societies 2019